AN INVESTIGATION OF THE DEVELOPMENT OF A MID-TROPOSPHERIC FRONTAL ZONE AND ITS ASSOCIATED VORTICITY FIELD

By Richard J. Reed and Frederick Sanders

Massachusetts Institute of Technology [1]

(Manuscript received 28 April 1953)

ABSTRACT

A synoptic example of intense frontogenesis at 500 mb is presented and the underlying mechanism is investigated both from the thermal and dynamic standpoints. It is shown that the basic process in operation is a cross-stream gradient of sinking motion with strongest subsidence at the warm edge of the frontal zone. This condition gives rise to an intensified horizontal temperature gradient and, because of the generally disregarded "vertical-shear" terms in the vorticity equation, leads to a marked increase in vorticity as well.

The Ertel vorticity theorem is applied in order to confirm the above conclusions and also to show that in certain regions the frontal zone was of stratospheric origin, the lower boundary being initially part of the polar tropopause.

Finally it is shown how the vertical-shear terms may be incorporated in the Sawyer-Bushby numerical prediction model.

1. Introduction

A distinct example of frontogenesis at the 500-mb level occurred during the period 1500 GCT 27 January 1953 to 0300 GCT 28 January 1953, as illustrated in figs. 1 and 2. From a precursory examination of reported temperatures, humidities and winds it appears that descending motion is present within the frontal zone with maximum subsidence near the warm edge. According to the frontogenetical equation of Miller (1948), such a cross-stream distribution of vertical motion tends to produce an increase in the horizontal temperature gradient of the frontal zone. Moreover, consideration of the complete vorticity equation reveals that these same motions tend to strengthen the cyclonic vorticity within the zone.

The possibility exists, therefore, that the frontogenesis, as regards both the temperature and wind fields, may be largely the result of the cross-stream variation of vertical motion. Since synoptic experience indicates that the January case is not an isolated phenomenon, but an unusually well-developed instance of a rather common occurrence, it appears desirable to investigate this case in greater detail. Thus quantitative estimates are made of all terms in the Miller expression to determine the role of the process in question in producing the intensification of the temperature gradient. Likewise, all terms in the complete vorticity equation are evaluated so that the importance of this mechanism in generating the increased cyclonic vorticity of the frontal zone may also be determined. Two facts lend confidence to the results of the measurements. First, the density of radiosonde, rawin and pilot-balloon reports (shown in part in figs. 1 and 2) was above average. Second, the development was so pronounced that considerable errors in the measurement of the various quantities could be present without altering the basic results.

2. Analysis of data

To provide a more detailed picture of the structure of the frontal zone, extensive use was made of all pertinent upper-level data. Analysis of radiosonde observations showed that significant changes in lapse rate in the same sense tended to occur at approximately the same potential temperature at all stations over a considerable area, leading to the conclusion that continuous surfaces of lapse rate discontinuity were present. Thus analyses were made of charts showing the pressure level and potential temperature of the more significant of these discontinuities. From these analyses the boundaries of the frontal zone were entered on the constant-pressure charts, and the isotherms in the vicinity of the zone were located as precisely as possible. The analyses of lapse rate discontinuities also provided the basis for the construction of the cross sections shown in figs. 3 and 4. Fig. 4 is chosen approximately normal to the strong portion of the frontal zone at the final time, while fig. 3 contains, at the initial time, the region of origin of the particles which were within the frontal zone near the 500-mb level at the later time. Additional aid in the drawing of these diagrams was obtained from analyses of temperature and contour height at the 700-mb, 500-mb, 400-mb and 300-mb levels.

[1] The research reported in this paper was sponsored by the Office of Naval Research, under Contract No. N5ori-07804, between the Office of Naval Research and the Division of Industrial Cooperation.

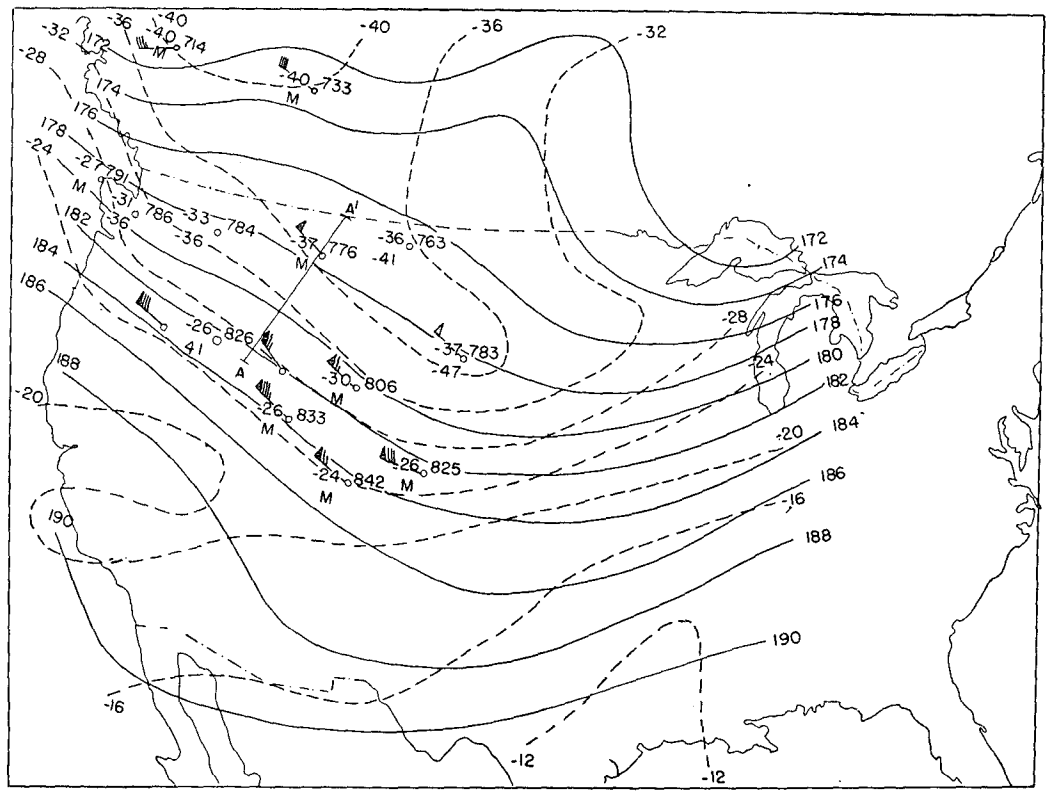

FIG. 1. 500-mb surface for 1500 GCT 27 January 1953 showing contours (thin solid lines) and temperatures (dashed lines). Observed radiosonde and rawin reports have been added in critical areas. Each half barb represents wind speed of 5 kn, each full barb 10 kn, and each solid wedge 50 kn. Contour height in ft and temperature in deg C.

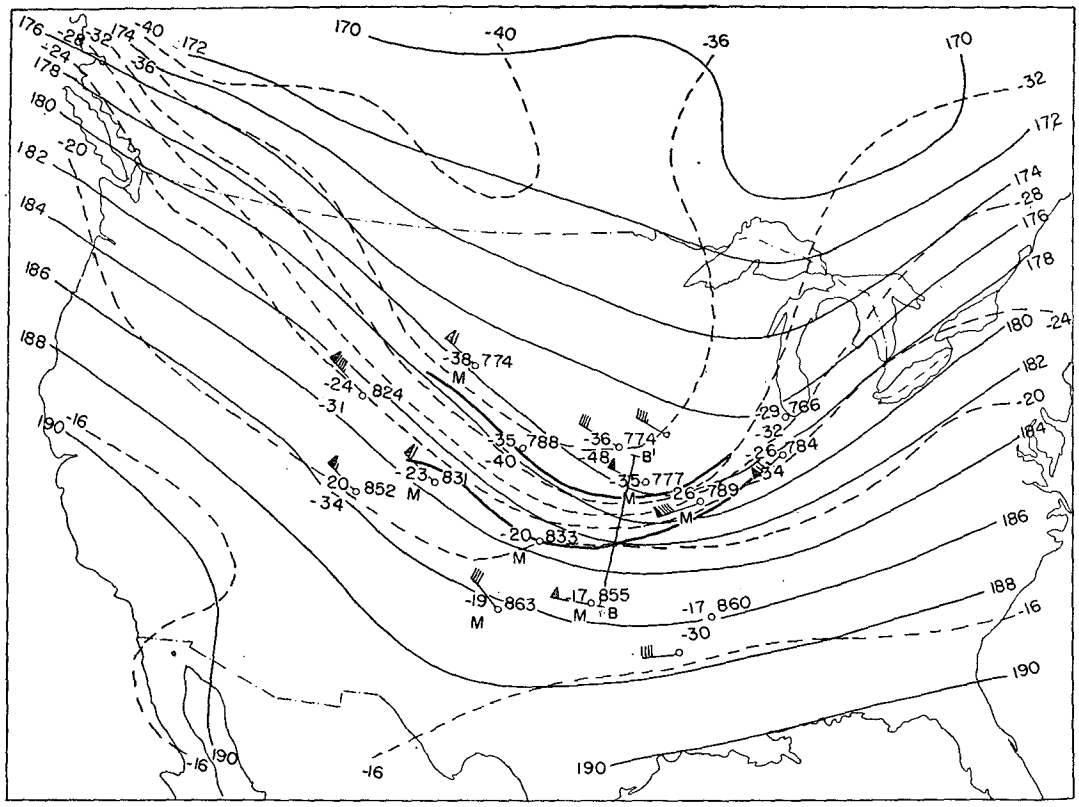

FIG. 2. 500-mb surface for 0300 GCT 28 January 1953. Heavy solid lines are frontal boundaries; otherwise representation is same as in fig. 1.

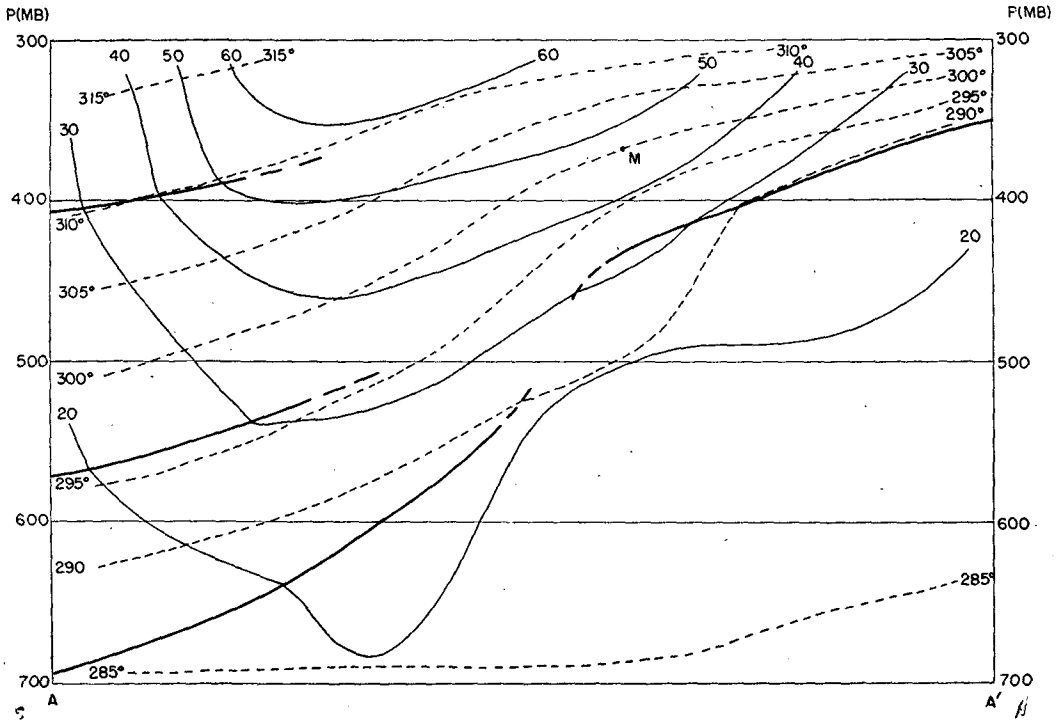

FIG. 3. Cross section along A—A′ in fig. 1. Thin solid lines give geostrophic wind speed (m/sec) normal to section; heavy solid lines are tropopause or frontal boundaries; dashed lines are isentropes.

The geostrophic wind components normal to the cross section were calculated by adding to the observed geostrophic components at 700 mb the increments given by the thermal wind equation in the form

$$\Delta u = -Rf^{-1} \ln (p_1/p_2)\, \overline{\partial T/\partial y}, \qquad (1)$$

where Δu is the change of normal wind component from pressure level p_1 to pressure level p_2, f is the Coriolis parameter, R the gas constant for air, and $\overline{\partial T/\partial y}$ is the mean horizontal temperature gradient within the layer from p_1 to p_2. In general, Δu was not computed between standard pressure levels but, to bring out the finer details of the wind structure, between frontal surfaces instead. Also, it should be noted that throughout this paper the x- and y-axes are taken, respectively, normal and parallel to the horizontal

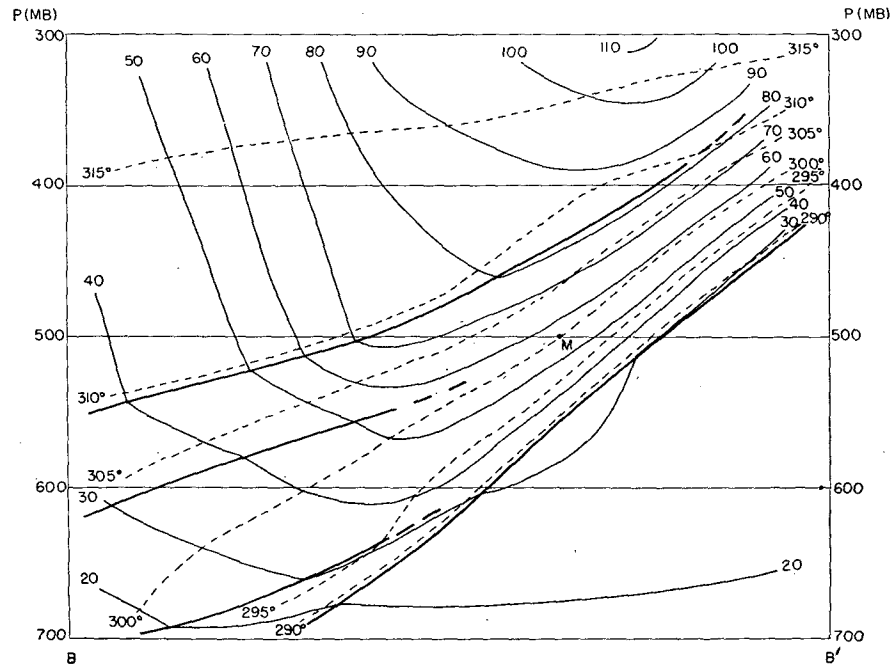

FIG. 4. Cross section along B—B′ in fig. 2. Notation as in fig. 3.

temperature gradient and normal to the flow in the middle and upper troposphere.

Vertical components of motion were determined by tracing trajectories of various air parcels. Because of the presence of strong vertical wind shear and the indications of sinking motion, it seemed both necessary and reasonable to utilize isentropic surfaces in calculating these trajectories, in a manner similar to that employed by Fleagle (1947). The surfaces chosen were those of 300K within the frontal zone, 293K and 307K near the cold and warm boundaries of the zone, respectively, and 284K and 315K, respectively, within the cold and warm air. The distribution of pressure on these surfaces was analyzed at the beginning and end of the 12-hr period under consideration, and was estimated for 2100 GCT 27 January, the middle of the period. Wind fields were analyzed on all of these charts, from observed reports supplemented where appropriate with geostrophic winds measured from the constant-pressure charts. Since the area studied was characterized by nearly straight flow, as can be seen in figs. 1 and 2, it was not generally necessary to compute gradient winds. After evaluation of the vertical motion from the individual change in pressure along each trajectory, this value was assumed to represent the instantaneous value at 2100 GCT at the midpoint of each trajectory. In this way analyses of vertical motion at each isentropic surface were performed from which an estimated cross section for 2100 GCT was prepared (fig. 5), extending approximately from Bismarck, N. D. to Pueblo, Colo. This line was chosen to contain the 2100-GCT position of the air parcels which terminated within the frontal zone at about 500 mb, in fig. 4. The normal wind components in fig. 5 were derived from the wind analyses for 2100 GCT, care being taken to render the vertical shear within the frontal zone consistent with that reported at relevant nearby stations. The quantities to be discussed below were taken largely from this 2100-GCT cross section.

3. Frontogenesis in the temperature field

It was decided to study frontogenesis following the three-dimensional motion since generative processes are of more interest physically than the mere transport of a pre-existing frontal zone from one level to another in the atmosphere. Accordingly, following Miller (1948), we may express the intensity of frontogenesis in the horizontal field by potential temperature by

$$-\frac{d}{dt}\left(\frac{\partial\theta}{\partial y}\right) = -\frac{\partial}{\partial y}\left(\frac{d\theta}{dt}\right) + \frac{\partial\bar{w}}{\partial y}\frac{\partial\theta}{\partial z} + \frac{\partial v}{\partial y}\frac{\partial\theta}{\partial y}, \quad (2)$$

where d/dt represents differentiation following the three-dimensional motion, and the y-axis is oriented

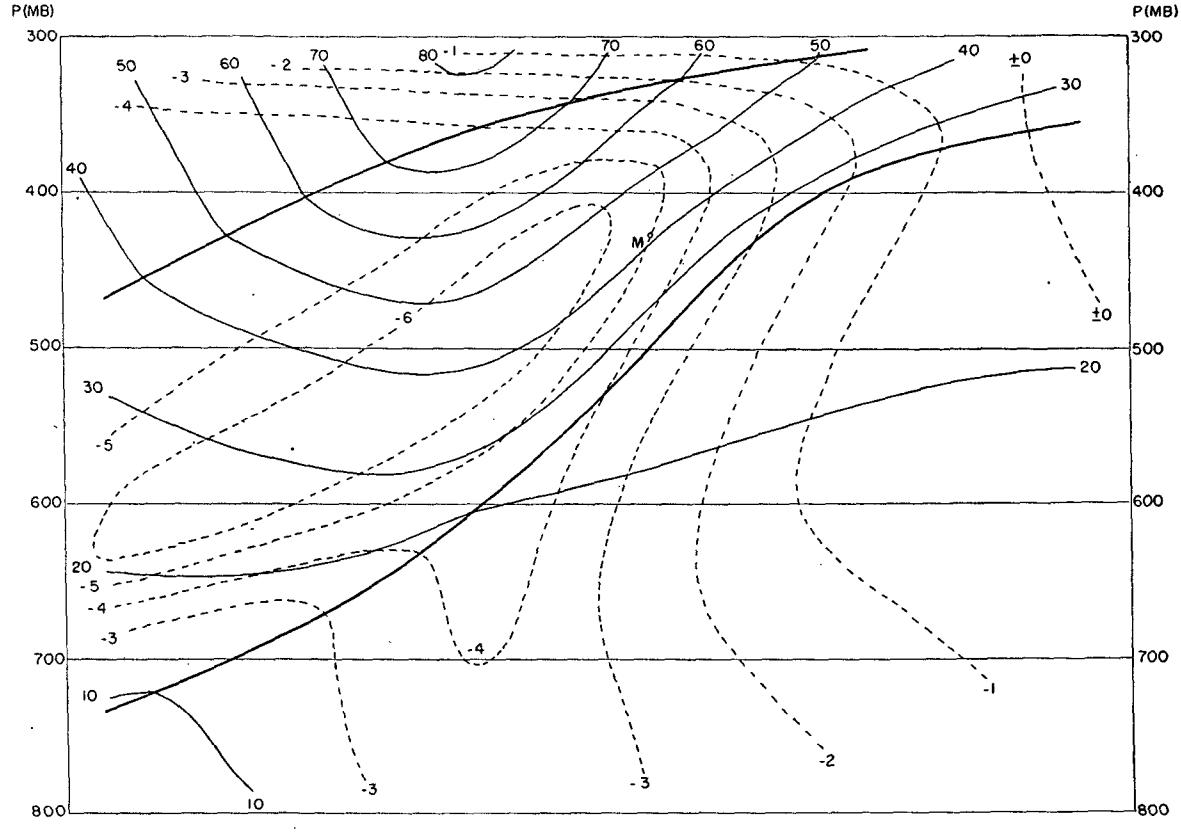

FIG. 5. Cross section from Bismarck, N. D. to Pueblo, Colorado at 2100 GCT 27 January 1953. Thin, solid lines give wind speed (m/sec); heavy, solid lines are frontal boundaries; dashed lines represent average 12-hr vertical velocities (cm/sec).

TABLE 1. Changes in temperature gradient at point M due to various terms in frontogenetical equation expressed in deg C per 100 km per 12 hr.

	$\Delta(-\partial\theta/\partial y)$
Tilting effect	+9
Confluence effect	−2
Total (computed)	+7
Total (observed)	+7
Two-dimensional (observed)	+9

parallel to the temperature gradient, directed toward colder air. The terms on the right-hand side of (2) may be described as follows: $-\partial(d\theta/dt)/\partial y$ is the non-adiabatic term, depending upon the horizontal variation of the non-adiabatic heating and cooling, which was disregarded in the present study; $(\partial w/\partial y)$ $(\partial\theta/\partial z)$ is the "tilting" term, which may be thought of as depending upon the horizontal variation of adiabatic heating and cooling arising from the horizontal gradient of vertical motion; and $(\partial v/\partial y)$ $(\partial\theta/\partial y)$ is the "confluence" term, representing the intensification of horizontal temperature gradient by horizontal motions alone.

The results of a computation of the magnitude of the above terms are presented in table 1, for a particle which terminates near the middle of the frontal zone at 500 mb (point M in fig. 4). The values were determined instantaneously at 2100 GCT and multiplied by the time interval to give the 12-hr changes shown in the table. It is quite clear that for this point the sole contribution to frontogenesis arises from the tilting term. Its effect is somewhat counterbalanced by the effects of the confluence term, which was actually tending to produce frontolysis. It should be added that the magnitude of the confluence effect could not be determined with much confidence owing to its great sensitivity to the details of the wind analysis, but its sign seems reasonably certain and furthermore the magnitude estimated from the 2100-GCT chart agreed reasonably well with the mean of the values at the beginning and end of the period. The fact that the observed change in frontal intensity was nearly equal to the sum of the measured effects also lends confidence to the entire analysis. Finally, it should be noted from table 1 that the change in horizontal temperature gradient along the three-dimensional trajectory is only slightly less than that along a two-dimensional trajectory at 500 mb. The difference between these changes may be thought of as a measure of the effect of downward vertical transport of horizontal temperature gradient in producing frontogenesis at the 500-mb level. Clearly this effect was small in the present instance.

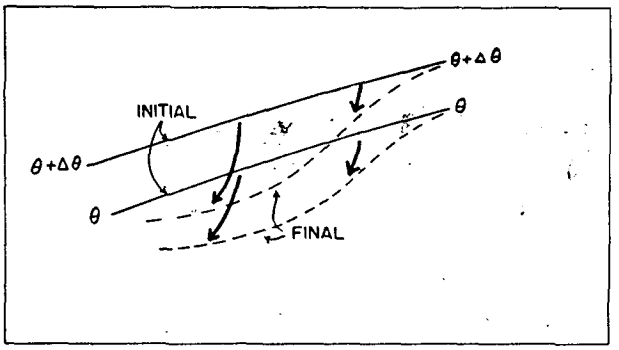

FIG. 6. Schematic diagram illustrating opposing effects of difluence and vertical motion in producing frontogenesis in temperature field. Solid lines show initial positions of isentropes (θ) in plane normal to flow; dashed lines show final position. Heavy arrows represent displacements of selected points on isentropic surfaces.

Examination of the charts and cross sections indicates that the results of the computations for point M are representative of those for all points within the frontal zone in the middle troposphere. Accordingly a schematic diagram is presented in fig. 6, showing how the tilting of the isentropic surfaces produces significant frontogenesis in the horizontal temperature field, despite a slight difluence in the horizontal motion.

4. Dynamic aspects of the frontogenesis

In a natural coordinate system, that is, in a system with the x-axis directed along the wind flow and the y-axis normal to it in a counter-clockwise sense, the vertical component of relative vorticity[2] may be expressed as $-\partial u/\partial y + u/r$, where u is the wind speed in the x direction and r the radius of curvature of the streamlines. Since the cross sections in both figs. 3 and 4 are chosen at right angles to the flow, the shearing component of vorticity $-\partial u/\partial y$ may be inferred from the diagrams. On the other hand, the curvature component u/r cannot be surmised directly. However it is evident from the shape of the 500-mb contours (figs. 1 and 2) that only slight curvature is present along both sections. To a first approximation, therefore, the curvature term may be neglected in zones of large horizontal wind shear appearing on the cross sections, and the total vorticity may be measured from the wind shear alone. Making use of this approximation to estimate the vorticity within the frontal zone, we note from a comparison of figs. 3 and 4 that a remarkable increase in cyclonic vorticity occurs between 1500 GCT 27 January and 0300 GCT 28 January. The mechanism responsible for this rapid generation of vorticity will now be investigated.

Sutcliffe (1947) has shown that in a coordinate system with pressure as vertical coordinate, the vorticity equation may be written

$$\frac{d\zeta_p}{dt} = (\zeta_p + f)\frac{\partial}{\partial p}\left(\frac{dp}{dt}\right) + \frac{\partial u}{\partial p}\frac{\partial}{\partial y}\left(\frac{dp}{dt}\right) - \frac{\partial v}{\partial p}\frac{\partial}{\partial x}\left(\frac{dp}{dt}\right) - \frac{df}{dt}. \quad (3)$$

[2] Afterward referred to simply as "vorticity."

In this equation, u and v are the horizontal wind components in the x (east) and y (north) directions, respectively; p is pressure, f is the Coriolis parameter, and $\zeta_p = (\partial v/\partial x)_p - (\partial u/\partial y)_p$ is the isobaric vorticity, or the vorticity measured on a constant pressure surface.

In cases of significant vertical motion, such as the one dealt with here,

$$dp/dt \approx w\,\partial p/\partial z = -g\rho w, \tag{4}$$

where g is the acceleration of gravity, ρ the air density and w the vertical velocity. Substitution of (4) in (3) gives

$$\frac{d\zeta_p}{dt} = -g\left[(\zeta_p + f)\frac{\partial}{\partial p}(\rho w) + \frac{\partial u}{\partial p}\frac{\partial}{\partial y}(\rho w) - \frac{\partial v}{\partial p}\frac{\partial}{\partial x}(\rho w)\right] - \frac{df}{dt}. \tag{5}$$

The first term on the right hand side of (5) is analogous to the divergence effect in the more familiar form of the vorticity equation, and will hereafter be referred to as the "divergence" term. The second and third terms represent the effect of a horizontal gradient of vertical velocity in transforming vorticity about a horizontal axis to that about a vertical axis. In future reference these will be called the "vertical-shear" terms. The change in vorticity arising from latitudinal displacement is expressed by the final term. Because of the prominence given this term in theoretical works of Rossby, it will be referred to as the "Rossby" term.

Since rotation of the x- and y-axes, within a horizontal plane, does not change the form of (5), they may be chosen in any convenient orientation. In conformance with the convention adopted in section 2, the x-axis is pointed in the direction of flow. With this choice of axes, further simplification of (5) is possible in the present case, inasmuch as the following inequalities were observed to be true within the frontal zone:

$$\partial v/\partial p \ll \partial u/\partial p, \qquad \partial(\rho w)/\partial x \ll \partial(\rho w)/\partial y, \tag{6}$$

and

$$(\partial v/\partial x)_p \ll (\partial u/\partial y)_p.$$

Thus (5) reduces to

$$\frac{d}{dt}\left(-\frac{\partial u}{\partial y}\right)_p = -g\left\{\left[f - \left(\frac{\partial u}{\partial y}\right)_p\right]\frac{\partial}{\partial p}(\rho w) + \frac{\partial u}{\partial p}\frac{\partial}{\partial y}(\rho w)\right\} - \frac{df}{dt}. \tag{7}$$

Equation (3) is now in a form suitable for determination of the respective roles of the divergence, vertical shear and Rossby terms in generating the cyclonic vorticity of the frontal zone. The graphical methods developed by V. Bjerknes (1911) were employed in carrying out the indicated additions, multiplications and differentiations. Since the horizontal variation of density was small compared with that of other quantities in (7), mean values were assumed at the various pressure levels. Values of u and w were taken from fig. 5. Thus derivatives of u are instantaneous values in the middle of the 12-hr period, while derivatives of w are average values for the entire period. The measurements based on (7) were regarded as averages for the 12-hr interval, and were multiplied by the time interval in order to give the 12-hr vorticity changes depicted in figs. 7, 8, 9 and 10.

These figures reveal several points of interest. Most significant perhaps is the fact that in the region between 400 and 500 mb the vertical-shear term or tilting effect is almost entirely responsible for the increased cyclonic vorticity. The divergence term actually tends to produce a slight decrease in this same region, while a slight increase results from the Rossby effect. At higher and lower levels the convergence term predominates, producing a large increase in cyclonic vorticity in the vicinity of 300 mb, and a substantial decrease on the cold side of the frontal zone at 700 mb and a lesser increase on the warm side. These changes agree well with Palmén's observation (1948) that as a rule "within the frontal layer the cyclonic shear is weakest near the 700-mb level and strongest near the northernmost upper extension of the frontal layer." Of the three mechanisms considered, it is apparent that the Rossby effect is least instrumental in producing vorticity change.

Restricting our attention now to the principal aim of the present paper—the explanation of the frontogenesis at the 500-mb level, we examine the processes responsible for the observed growth of vorticity at that level. As in the preceding section, where the thermal aspects of the frontogenesis were investigated, the important question in this respect is: what was the vorticity change on the air parcel M, which terminated in the frontal zone at 500 mb (fig. 4), and how was this change divided among the components in (7)? To answer this question it is necessary to consider the mid-point of the trajectory, point M in figs. 7, 8, 9 and 10. Table 2 summarizes the indicated vorticity changes. From the table it can be seen that in the

TABLE 2. Changes in vorticity at point M due to various terms in the vorticity equation expressed in sec^{-1} per 12 hr.

	$\Delta\zeta$
Divergence effect	-2×10^{-5}
Vertical-shear effect	+13
Rossby effect	+ 1
Total (computed)	+12
Total (observed)	+13
Two-dimensional (observed)	+18

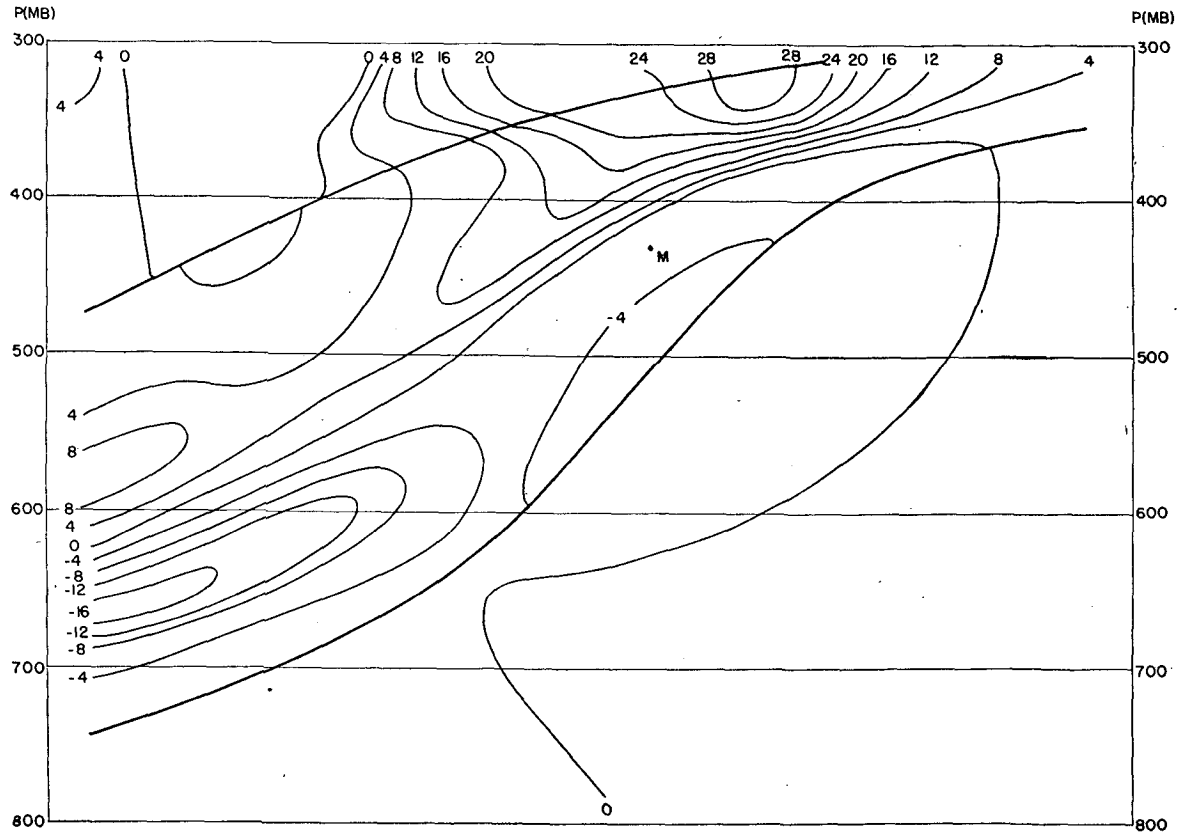

FIG. 7. Computed 12-hour vorticity change (thin lines) between 1500 GCT January 27 and 0300 GCT January 28 due to divergence effect only. Values must be multiplied by 10^{-5} sec^{-1}. Heavy lines are frontal boundaries.

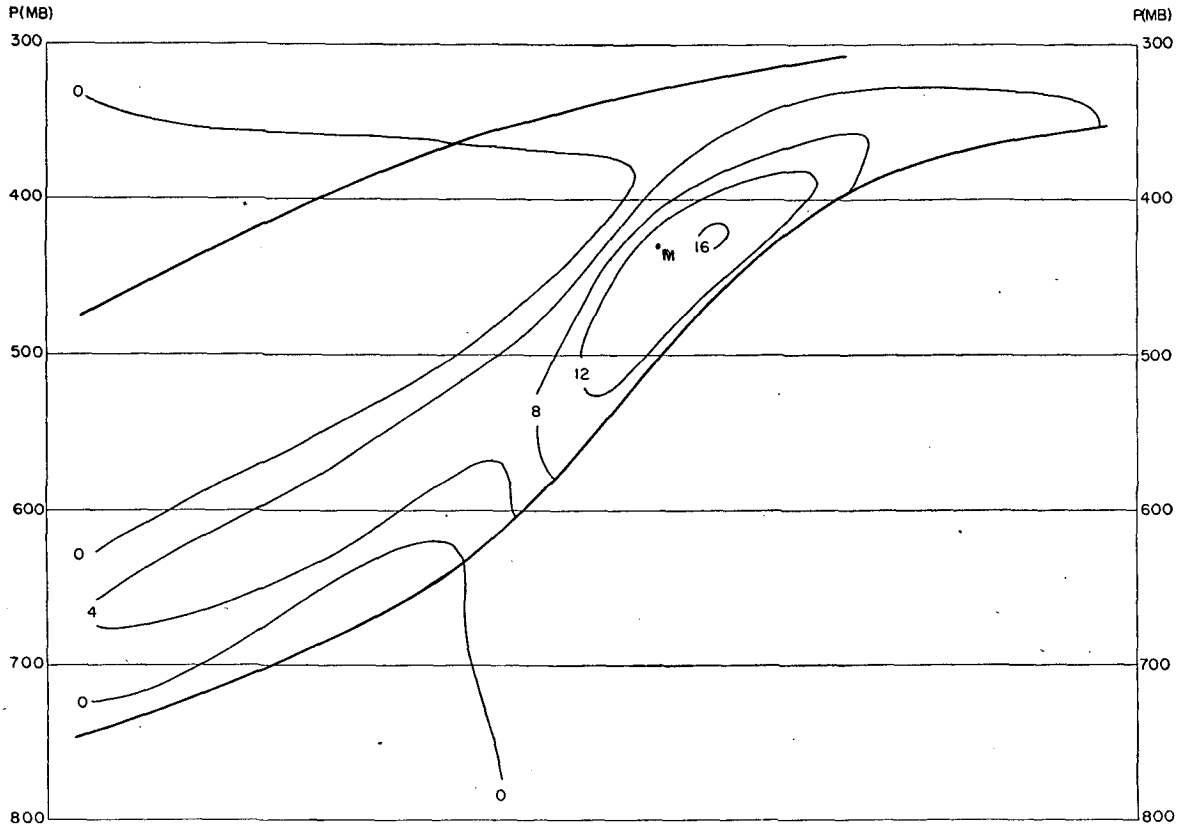

FIG. 8. Computed 12-hour vorticity change (thin lines) between 1500 GCT January 27 and 0300 GCT January 28 due to vertical shear effect only. Values must be multiplied by 10^{-5} sec^{-1}. Heavy lines are frontal boundaries.

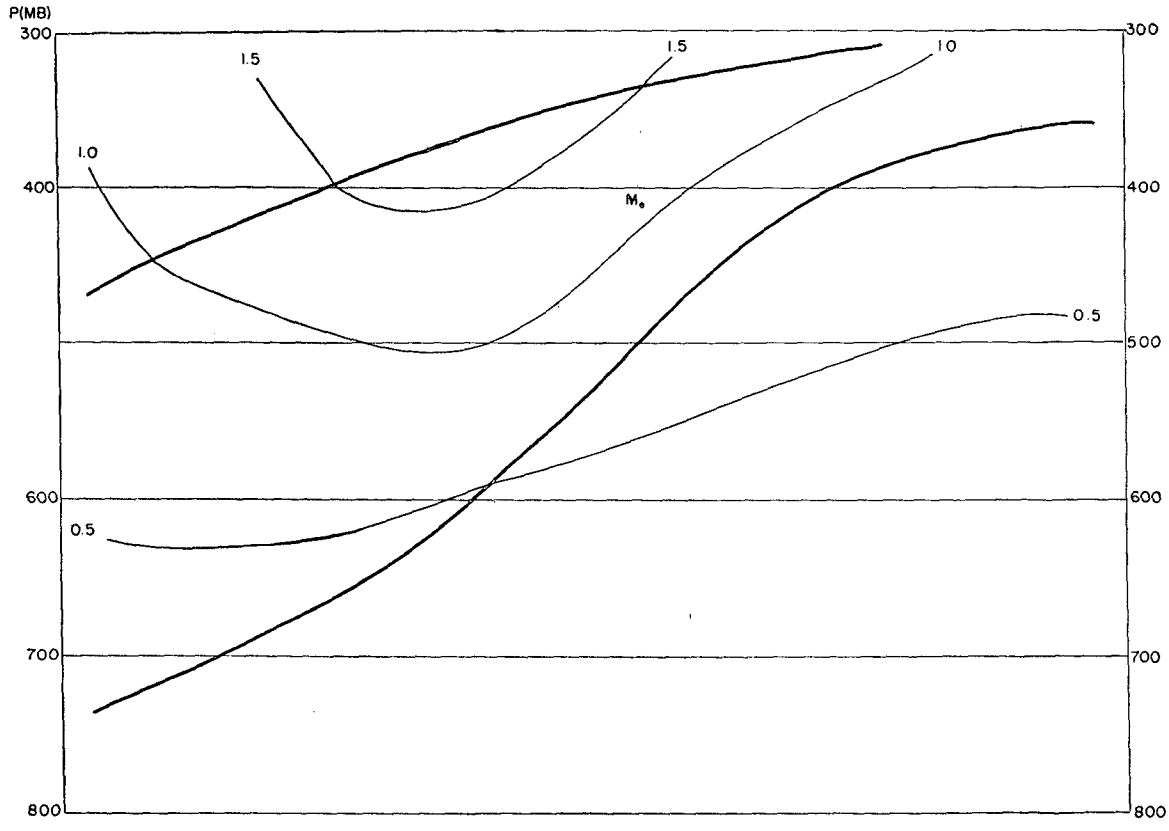

FIG. 9. Computed 12-hour vorticity change (thin lines) between 1500 GCT January 27 and 0300 GCT January 28 due to Rossby effect. Value must be multiplied by 10^{-5} sec^{-1}. Heavy lines are frontal boundaries.

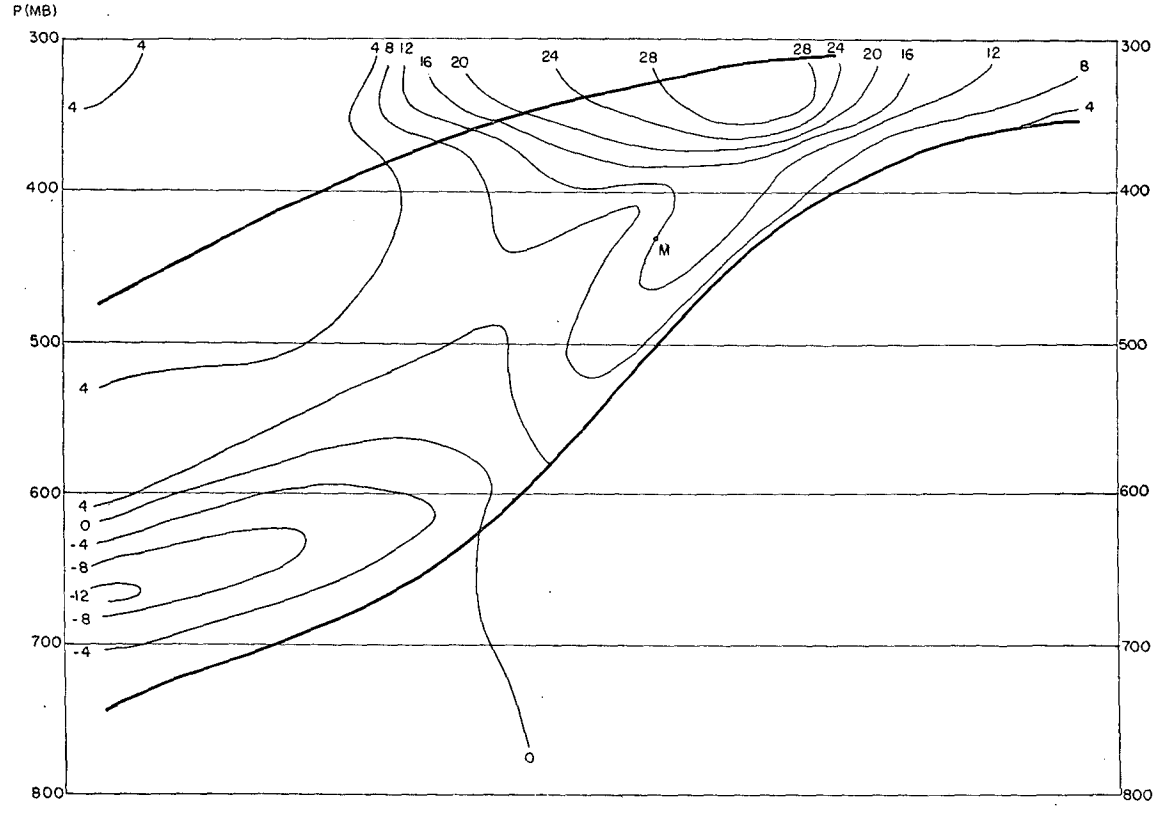

FIG. 10. Computed total 12-hour vorticity change (thin lines) between 1500 GCT January 27 and 0300 GCT January 28. Values must be multiplied by 10^{-5} sec^{-1}. Heavy lines are frontal boundaries.

case of the vorticity too, it is the tilting effect which is of paramount importance. The convergence gives a small negative contribution to the vorticity change, and the Rossby effect a small positive change. Also included in table 2 is the vorticity change at 500 mb following the horizontal motion only. This is somewhat greater than the change following the particle, indicating that the vorticity increase, as seen on successive 500-mb charts, must be ascribed in some measure to a downward transport of pre-existing vorticity, though the major change is due to the generative process.

The fact that in the case under consideration the vertical-shear term in (7) is found to exert the controlling influence on vorticity changes in the middle troposphere is not too surprising. Many years ago Fujiwhara (1923) speculated as to its possible importance in frontal phenomena. Hesselberg and Friedman (1914) in their classic measurements found it to be of equal magnitude as the divergence effect. More recently Reed (1951) has presented a synoptic example in which it was shown to be of significance. Bjerknes (1951) has advanced theoretical arguments for considering its role in vorticity changes.

Generally speaking, however, the vertical-shear terms have received little attention in problems relating to vorticity change. The results presented here suggest that they may well be deserving of more consideration, especially as regards upper-level frontal zones. Of course the question may be raised as to how much weight should be attached to the results of a single case study. Without further evidence it is conceivable that we are dealing, in the present instance, with an isolated or unusual synoptic situation. The writers feel that the case under consideration is unusual, but only in the sense of being extremely well developed. Examination of several months of 500-mb charts from the M.I.T. files revealed numerous instances where the same process was detectable by visual inspection alone. An equally remarkable example was evident on 20 October 1952 over northeastern United States. Among other cases of lesser intensity were the following:

27 October 1952 over eastern United States,
21 November 1952 over southeastern United States,
6 January 1953 over north central United States,
8 January 1953 in the Texas area,
20 January 1953 in the Colorado area,
17 February 1953 over southeastern United States,
19 February 1953 on the West Coast, and
24 February 1953 over southwestern United States.

The sequence of events at the surface which accompanies this case of upper-level frontogenesis warrants some comment. At the initial time significant surface frontogenesis, with associated cloudiness and some precipitation, is occurring along a line between western Kentucky and north central Texas. A weak cyclone on this front in eastern Oklahoma is moving eastward at about 30 kn with no significant change in intensity. In the subsequent twelve hours, it moves east-northeastward at the greatly accelerated speed of about 60 kn, while the central pressure drops about seven mb. These prominent changes near the ground occur simultaneously with the upper-level frontogenesis and at some distance to the east.

5. Application of Ertel's vorticity theorem

The results of the preceding sections have indicated a simple physical picture of the creation of the mid-tropospheric frontal zone. The basic mechanism was discovered to be a cross-stream distribution of sinking motion, such that strongest subsidence occurred on the right-hand (or warm) edge of the current, facing downstream. The accompanying cross-stream variation in adiabatic warming gave rise to the intensified temperature gradient. At the same time, the observed vertical motions, again facing downstream, produced a clockwise rotation of an initially horizontal axis so that the cyclonic vertical wind shear acquired a component about a vertical axis. This process was manifested by a sharp increase in the vorticity of the frontal zone.

As a check on the correctness of this picture and also for the purpose of introducing a very useful method of analysis, we will now consider a vorticity theorem first derived by Ertel (1942). This theorem is especially suited to the present investigation since it combines in one equation the three-dimensional frontogenetical expression of Miller (1948), the vorticity equation in three dimensions and the equation of continuity. The Ertel theorem states that for adiabatic, frictionless motion the following relationship holds:

$$\frac{d}{dt}[\sigma(\boldsymbol{Z} + 2\boldsymbol{\Omega})\cdot\nabla\theta] = 0, \tag{8}$$

where σ is the specific volume, $\boldsymbol{Z}$ is the three-dimensional vorticity vector, $\nabla \times \boldsymbol{V}$, and $\boldsymbol{\Omega}$ is the earth's rotation vector.

By a transformation of coordinates, it can be shown that (8) may be written

$$(\zeta_\theta + f)\frac{\partial\theta}{\partial p} = C, \tag{9}$$

where $\zeta_\theta = (\partial v/\partial x)_\theta - (\partial u/\partial y)_\theta$, the vorticity measured on a potential temperature surface, and C is a constant. Alternatively (8) may be written

$$(\zeta_p + f)\frac{\partial\theta}{\partial p} + \boldsymbol{k}\cdot\frac{\partial \boldsymbol{V}}{\partial p} \times \nabla_p\theta = C. \tag{10}$$

In this equation, $\boldsymbol{k}$ is the unit vertical vector, $\boldsymbol{V}$ the horizontal wind vector and $\nabla_p\theta$ denotes the potential

temperature gradient measured on a constant pressure surface. Since, strictly speaking, only the point M in figs. 3 and 4 is contained in the plane of the cross section, further remarks will be confined to this point. In both sections $-\partial u/\partial y_\theta$ at M is very slight, and, as noted in previous sections, the curvature component of vorticity is small, too. It follows therefore that $\zeta_\theta + f$ changed little during the 12-hr period. The figures also reveal that the change in $\partial\theta/\partial p$ was negligible. Thus (9) above is satisfied, attesting to the accuracy of the analyses in the regions considered.

Next, applying (10), we find that $\nabla_p\theta$ at M is nearly doubled in value and, in accordance with the thermal wind equation, $\partial V/\partial p$ behaved likewise. Consequently the second term in (10) experienced an almost fourfold increase during the 12 hours. As before, $\partial\theta/\partial p$ remained approximately constant, so in order for (9) to balance, a strong increase in $\zeta_p + f$ was necessitated. Examination of the figures clearly shows this increase. Quantitatively it was found that $\zeta_p + f$ should have doubled. The actual increase was somewhat less, but in view of the approximations involved the verification is satisfactory. No attempt was made to apply (9) and (10) to large areas of the map, but the preceding example of their application at a single key point illustrates their usefulness as a tool in the study of frontogenesis.

6. Further development

During the 12-hr period following 0300 GCT 28 January, intensification of the frontal zone continued. The extraordinary high-level frontal zone present at 1500 GCT on the 28th is demonstrated by the PIT and FFO radiosonde and rawin observations, represented in fig. 11. From the geometry of the situation the frontal intensity is measured as 11C per 50 km, a value comparable to that of the strongest surface fronts. The vorticity is also extreme, 40×10^{-5} sec^{-1}, or four times the Coriolis parameter in the latitude of the cross section.

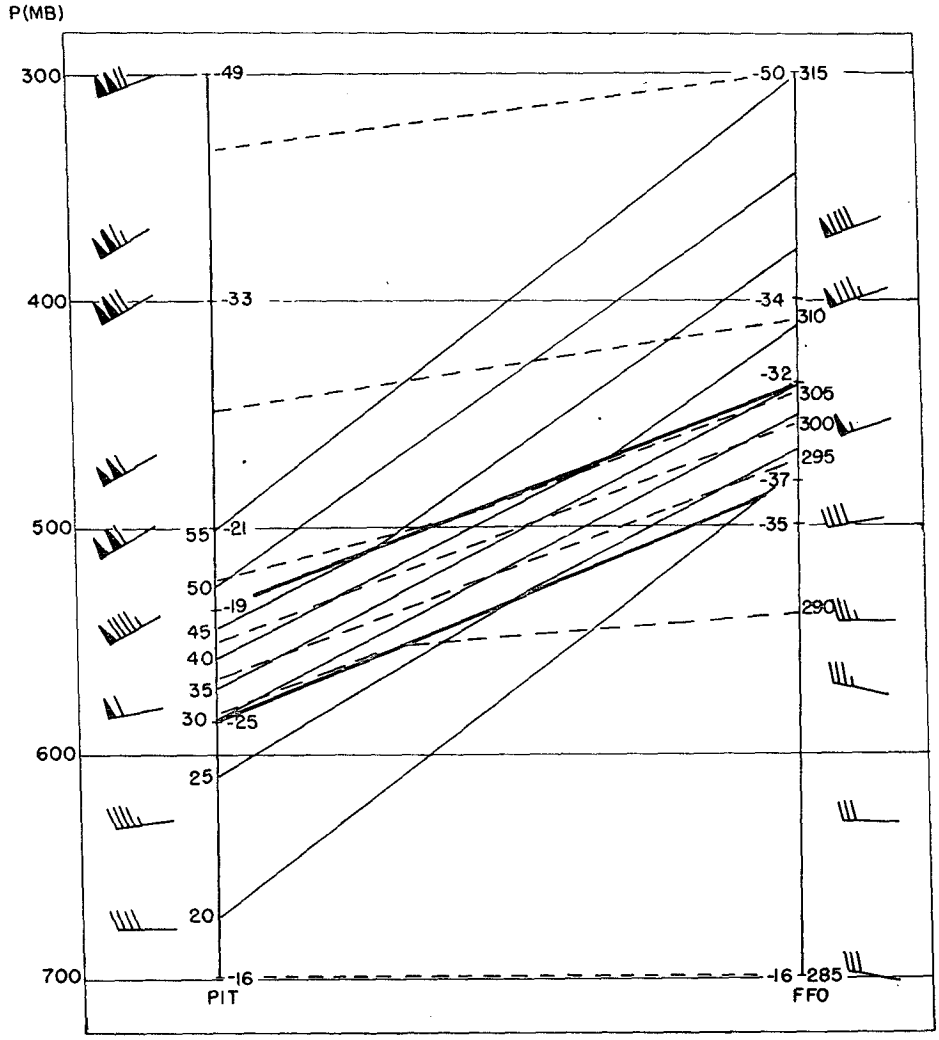

FIG. 11. Cross section from Pittsburgh, Pa. (PIT) to Dayton, Ohio (FFO) showing intense high-level frontal zone at 1500 GCT 28 January 1953. Thin solid lines give actual wind speeds (m/sec); heavy solid lines are frontal boundaries. Thin dashed lines are isentropes. Temperatures are entered on inner side of verticals. Observed winds are included in margins according to convention explained in legend to fig. 1.

The purpose in presenting this figure, however, is not so much to illustrate the frontal structure or to confirm the previous frontal analysis, as to call attention to an additional point of interest. From careful examination of fig. 11, it appears that the product $(\zeta_\theta + f)\ (\partial\theta/\partial p)$ in the frontal zone at this time is greater than it was anywhere on the previous section. Consideration of the areas outside of the earlier section discloses that in order for (9) to be obeyed, the air in question must have its origin to the north of this section (fig. 4). Soundings in these more northerly regions are all similar, displaying relatively steep lapse rates in the troposphere separated from approximately isothermal conditions in the stratosphere by a low, distinct polar tropopause. On these soundings only the air in the lower stratosphere was sufficiently stable for (9) to be satisfied. Moreover the potential temperature at the polar tropopause was within a few degrees of that at the base of the frontal inversion at PIT and FFO. The conclusion seems almost inescapable that the frontal zone was in fact a portion of the lower stratosphere which underwent strong subsidence with the tropopause assuming the character and appearance of a frontal surface. The northern portion of the frontal zone at 0300 GCT on the 28th seems likewise to have been stratospheric air at the initial period (1500 GCT on the 27th).

7. An application to numerical prediction

Until now most numerical prediction models have been based on the simplified vorticity equation,

$$d(\zeta + f)/dt = -(\zeta + f)\ (\partial u/\partial x + \partial v/\partial y). \quad (11)$$

In the most primitive models the divergence term is neglected; this procedure being justified by performing computations at the so-called "level of non-divergence." The present investigation, however, has shown that in certain cases the vertical-shear terms in the complete vorticity equation (3) are of appreciable magnitude at precisely that level, and that even in regions of strong divergence they are not always negligible. It is desirable, therefore, to include these terms in numerical models, if such a course is feasible. In the present section it will be shown that these terms may be incorporated in one numerical prediction scheme—the Sawyer-Bushby model (1953)—without adding significant complication.

In this model three equations are derived in three dependent variables: h_m, h' and $\Pi = dp/dt$. Here h_m is the height of the central pressure p_m of the layer bounded near the top of the atmosphere by $p = p_1$ and near the bottom by $p = p_0$; h' is the thickness of the layer from $p = p_0$ to $p = p_m$. For the sake of convenience, a vertical coordinate α is chosen according to the definition

$$\alpha = (p_0 + p_1 - 2p)/(p_0 - p_1). \quad (12)$$

A basic assumption of the model is that the thermal wind is constant in direction in any vertical column, and that it is proportional to the pressure interval. Accordingly,

$$V_g = V_{gm} + \alpha V_g', \quad \zeta_g = \zeta_{gm} + \alpha\zeta_g'; \quad (13)$$

the subscript g referring to geostrophic conditions and m to values at the pressure level $\frac{1}{2}(p_0 + p_1)$. V_g' represents the thermal wind from pressure level p_0 to p_m, and ζ_g' is the vorticity of the thermal wind.

Two of the three equations in the Sawyer-Bushby model are based on (11). The first of these is called the development equation, and is obtained by taking the difference between the vorticity equation applied at $p = p_1$ and $p = p_0$. The second is termed the equation of mean motion and is derived by integrating the vorticity equation between $p = p_0$ and $p = p_1$. Since the model contains the further assumption that

$$\Pi = \Pi_m(1 - \alpha^2), \quad (14)$$

it follows that $\Pi = 0$ at $p = p_0$ and $p = p_1$, and hence $\partial\Pi/\partial x$ and $\partial\Pi/\partial y = 0$ also. As a result the vertical shear terms,

$$(\partial u/\partial p)\ (\partial\Pi/\partial y) - (\partial v/\partial p)\ (\partial\Pi/\partial x), \quad (15)$$

disappear from the development equation, even when the complete vorticity equation is employed, and the Sawyer-Bushby model remains unchanged in this respect.

Considering next the equation of mean motion, we note first that

$$\partial/\partial p = -2(p_0 - p_1)^{-1}\ \partial/\partial\alpha. \quad (16)$$

In view of this relationship and (13) above,

$$\frac{\partial u}{\partial p}\frac{\partial \Pi}{\partial s} = -\frac{2}{p_0 - p_1}u'\frac{\partial \Pi}{\partial s},$$

and

$$\frac{\partial v}{\partial p}\frac{\partial \Pi}{\partial r} = -\frac{2}{p_0 - p_1}v'\frac{\partial \Pi}{\partial r}, \quad (17)$$

where now, following Sawyer and Bushby, curvilinear distance coordinates r and s, are used in place of x and y.

Integration of (15) between $\alpha = -1$ and $\alpha = +1$, under the assumption in (14), gives

$$\begin{aligned}\int_{-1}^{1}\left(\frac{\partial u}{\partial p}\frac{\partial \Pi}{\partial s} - \frac{\partial v}{\partial p}\frac{\partial \Pi}{\partial r}\right)d\alpha &= -\frac{2}{p_0 - p_1}\int_{-1}^{1}\left(u'\frac{\partial \Pi}{\partial s} - v'\frac{\partial \Pi}{\partial r}\right)d\alpha \\ &= \frac{2u'}{p_0 - p_1}\frac{\partial \Pi_m}{\partial s}\int_{-1}^{1}(1 - \alpha^2)\,d\alpha \\ &\quad + \frac{2v'}{p_0 - p_1}\frac{\partial \Pi_m}{\partial r}\int_{-1}^{1}(1 - \alpha^2)\,d\alpha \\ &= -\frac{8}{3(p_0 - p_1)}\left(u'\frac{\partial \Pi_m}{\partial s} - v'\frac{\partial \Pi_m}{\partial r}\right). \quad (18)\end{aligned}$$

Finally, from the geostrophic relationship and the definition of u' and v', it follows that

$$u' = -(g/f)\,(\partial h'/\partial s), \quad v' = (g/f)\,(\partial h'/\partial r), \quad (19)$$

and therefore (18) becomes

$$-\frac{8}{3(p_0 - p_1)}\left(u'\frac{\partial \Pi_m}{\partial s} - v'\frac{\partial \Pi_m}{\partial r}\right) = \frac{8g}{3f(p_0 - p_1)}\left(\frac{\partial h'}{\partial s}\frac{\partial \Pi_m}{\partial s} + \frac{\partial h'}{\partial r}\frac{\partial \Pi_m}{\partial r}\right). \quad (20)$$

Equation (20) may in turn be multiplied by f/g and combined with the term

$$8\Pi_m \nabla_s^2 h'/3(p_0 - p_1) \quad (21)$$

in the Sawyer-Bushby equation of mean motion to give

$$\frac{8\Pi_m}{3(p_0 - p_1)}\nabla_s^2 h' + \frac{8}{3(p_0 - p_1)}(\nabla h' \cdot \nabla \Pi_m) = \frac{8}{3(p_0 - p_1)}\nabla \cdot (\Pi_m \nabla h'). \quad (22)$$

With (22) now substituted for (21), the Sawyer-Bushby equations become:

$$\nabla^2 \frac{\partial h'}{\partial t} + J(h_m, \beta^2 g f^{-1}\nabla^2 h') + J(h', \beta^2 g f^{-1}\nabla^2 h_m + f) = \frac{4\Pi_m(\nabla^2 h_m + f^2/\beta^2 g)}{p_0 - p_1}, \quad (23)$$

$$\nabla^2 \frac{\partial h_m}{\partial t} + J(h_m, \beta^2 g f^{-1}\nabla^2 h_m + f) + \tfrac{1}{3}J(h', \beta^2 g f^{-1}\nabla^2 h') - \frac{8}{3(p_0 - p_1)}\nabla \cdot (\Pi_m \nabla h') = 0, \quad (24)$$

$$\partial h'/\partial t = \beta^2 g f^{-1} J(h', h_m) - RA\Gamma_p \Pi_m / g, \quad (25)$$

where J is the plane Jacobian operator and β the magnification factor $\sec^2 \frac{1}{2}(-\theta + \pi/2)$, and θ is the latitude.

As outlined by Sawyer and Bushby, the above equations can be solved by relaxation techniques. The only term affected by taking the vertical-shear terms into account is the final one in (24), and this in such a way that no change in the method of solution results. Since, in addition, little added labor is involved in calculating the quantity on the right hand side of (22), rather than the first term on the left, it would appear worthwhile to make use of the more exact expression in carrying out future computations.

Acknowledgments.—The authors wish to thank Professor J. M. Austin for helpful suggestions and criticisms and Miss I. Kole for the preparation of the diagrams.

REFERENCES

1. Bjerknes, J., 1951: Extratropical cyclones. *Compendium of meteorology*, Boston, Amer. Meteor. Soc., 577–599.
2. Bjerknes, V., 1911: *Dynamic meteorology and hydrography, Part II—kinematics.* Washington, Carnegie Institution, 175 pp.
3. Ertel, H., 1942: Ein neuer hydrodynamischer Wirbelsatz. *Meteor. Z.*, **59**, 277–281.
4. Fleagle, R. G., 1947: The fields of temperature, pressure and three-dimensional motion in selected weather situations. *J. Meteor.*, **4**, 165–185.
5. Fujiwhara, S., 1923: On the mechanism of extratropical cyclones. *Quart. J. r. meteor. Soc.*, **49**, 105–117.
6. Hesselberg, T., and A. Friedmann, 1914: Die Grossenordnung der meteorolozische Elemente und ihre raumlichen und zeitlichen Ableitungen. *Veroff. geophys. Inst. Univ. Leipzig*, **6**, 147–173.
7. Miller, J. E., 1948: On the concept of frontogenesis. *J. Meteor.*, **5**, 169–171.
8. Palmén, E., and C. W. Newton, 1948: A study of the mean wind and temperature distribution in the vicinity of the polar front in winter. *J. Meteor.*, **5**, 220–226.
9. Reed, R. J., 1951: A study of atmospheric vorticity. *Tech. Rep.* to ONR, Mass. Inst. Tech., 19 pp.
10. Sawyer, J. S., and F. H. Bushby, 1953: A baroclinic model atmosphere suitable for numerical integration. *J. Meteor.*, **10**, 54–59.
11. Sutcliffe, R. C., 1947: A contribution to the problem of development. *Quart. J. r. meteor. Soc.*, **73**, 370–383.